Broadband Electromagnetic Absorbing Structures Made of Graphene/Glass-Fiber/Epoxy Composite

Fabrizio Marra, Julian Lecini, Alessio Tamburrano, *Senior Member, IEEE*, Luigi Pisu, and Maria Sabrina Sarto, *Fellow, IEEE*

***Abstract*— Radar-absorbing structures (RASs) with improved mechanical properties and subwavelength thickness are of particular interest for aerospace applications and electromagnetic (EM) interference control. This article proposes a new RAS, made of a graphene-filled lossy laminate (LL) with impedance adapter, having a total thickness less than 4 mm and a normalized absorption bandwidth of 84% in the frequency range 6–18 GHz. The RAS is designed by applying an innovative simulation approach of the graphene-filled LL, which is based on the multiscale Maxwell Garnett model and the effective medium theory. Experimental tests are performed in order to validate the developed model and to assess the absorption properties of the produced RAS, having a minimum reflection of −30 dB and an absorption bandwidth at −10 dB of 10 GHz, with a central frequency of 12 GHz and a graphene nanoplatelets concentration less than 5 g/m^2.**

***Index Terms*— Composite materials, electromagnetic (EM) absorbers, graphene, graphene nanoplatelets (GNPs), radar-absorbing structures (RASs).**

I. Introduction

DURING the last decade, the development of multifunctional radar-absorbing structures (RASs) made of fiber-reinforced polymer composite, serving as electromagnetic (EM) absorber with structural properties, has been the focus of numerous studies [1]–[4]. The microwave absorption performance of conventional RASs has been noted to be improved by the dispersion of a high weight percent (wt%) of carbon-based nanofillers in a polymer matrix [5]–[9].

However, the implemented methods reported so far have several disadvantages and limitations in terms of fabrication, performance, and practical applicability at industrial scale, because of high viscosity and inhomogeneous mechanical and electrical properties mainly arising from the formation of nanofiller agglomeration and nonuniform distribution.

Manuscript received December 21, 2018; revised July 29, 2019; accepted October 10, 2019. Date of publication December 25, 2019; date of current version January 31, 2020. This work was supported by LEONARDO S.p.A. through the VELOGRAF Project. *(Corresponding author: Fabrizio Marra.)*

F. Marra, J. Lecini, A. Tamburrano, and M. S. Sarto are with the Department of Astronautics, Electrical and Energy Engineering, Sapienza University of Rome, 00185 Rome, Italy (e-mail: fabrizio.marra@uniroma1.it; julian.lecini@gmail.com; alessio.tamburrano@uniroma1.it; mariasabrina.sarto@uniroma1.it).

L. Pisu is with the Aircraft Division, Leonardo S.p.A., 10146 Turin, Italy (e-mail: luigi.pisu@ leonardocompany.com).

Color versions of one or more of the figures in this article are available online at http://ieeexplore.ieee.org.

Digital Object Identifier 10.1109/TMTT.2019.2950223

An extensive review on the use of carbon-based nanoreinforcement to improve the degradation properties of laminated continuous-fiber/epoxy composites is reported in [10]–[12].

Several studies have investigated the use of graphene nanoplatelets (GNPs) or graphene oxide (GO) as nanofiller in glass-fiber composite to improve the mechanical properties, without any focus on the electrical or EM performances. In [13], GO-filled epoxy resin at 0.25 wt% of GO was used to produce the glass-fiber composite through liquid resin infusion. The main difficulty of the process was to avoid the formation of nanofiller agglomerates along the fiber texture. A similar approach was investigated in [14], in which GO-filled epoxy resin was used to produce glass-fiber prepreg. GNPs as reinforcement in glass fiber/epoxy composites were proposed in [15]. GNPs were initially dispersed in isopropanol and then brushed over the glass fabric, which was then used to produce the laminate composite through vacuum-assisted resin transfer molding. In [16] and [17], the interfacial and mechanical properties of fiber-reinforced composites were improved through the use of GOs or GNPs as a filler.

The aforementioned studies are focused only on the improvement of the mechanical property of the composite and not on the EM absorbing characteristics, aimed at the development of an RAS. Actually, the production of structural fiber-reinforced composite laminates with radar absorbing properties is still an open issue because, in general, satisfactory structural performances are achieved only at nanofiller concentration much lower than that corresponding to an improvement of EM absorption properties. Moreover, a real challenge in stealth technology consists in the production of thin broadband absorbing screen, having a total thickness smaller than a quarter wavelength in free space at the central frequency of the range of interest, and characterized by an absorption bandwidth at −10 dB larger than 70% of the central frequency.

Sarto *et al.* [18], D'Aloia *et al.* [19], and Marra *et al.* [20] have developed broadband thin EM absorbing panel made of graphene-filled epoxy or vinyl ester composite, but the produced prototypes of radar-absorbing material (RAM) did not perform as RAS. More recently, an innovative process has been developed in order to realize thin broadband RAS with improved mechanical properties. The new fabrication method based on liquid resin infusion allowed to produce a glass-fiber-reinforced composite (GFC) laminate filled with GNPs with good structural properties. This was achieved through the prewetting of both faces of each glass fiber ply of the laminate

with a GNP-loaded sizing agent. The maximum absorption bandwidth at −10 dB of the produced panel was 68% and the panel thickness was 1 mm.

However, in order to optimize the absorption properties of the screen, the availability of simulation models that enable to predict the effective EM properties of the composite laminate is of crucial relevance.

The effective medium theory applied to carbon-fiber composite laminates was developed by Holloway *et al.* [21] for shielding applications. Polymer composites filled with short carbon fiber having a random distribution were modeled applying the Maxwell Garnett formalism in [4]. Nevertheless, in case of polymer composite filled with carbon nanostructures, such as carbon nanotubes (CNTs) or GNPs, a novel multiscale formulation of Maxwell Garnett effective medium model was proposed in [22] for GNP–epoxy composites and in [23] for GNP-coated aramid honeycomb panels.

The aim of this article is to propose an innovative approach to the design and fabrication of wideband RAS made of a graphene-loaded glass-fiber/epoxy composite laminate. To this purpose, we apply the technology described in [24] for the production of GFC panel made with GNP-coated glass-fiber plies. In particular, herewith, we develop and validate an innovative multiscale effective medium model of the GNP-loaded GFC laminate in order to design a broadband RAS for the range of 6–18 GHz by the simulation. The new absorbing screen consists of a GNP-loaded GFC laminate with impedance adapter (IA), and it is characterized by a normalized bandwidth larger than 80% and a total thickness of 15% the quarter wavelength at the central frequency. Such combined performances cannot be found elsewhere in the literature, as discussed in Section IV.

The multiscale effective medium model developed in this article is new because it considers the combined effects of GNP penetration through the glass-fiber spacing in each ply, GNP dispersion in the polymer prewetting agent, and lamination of the GNP-loaded glass-fiber plies.

The developed simulation model is validated through measurement and then applied for the RAS design. The absorbing screen is fabricated through vacuum-assisted liquid resin infusion with a total GNP content lower than 1 wt%. The reflection coefficient of the produced panel is measured in free space for normal incidence.

II. Fabrication of Graphene-Filled RAS

A. RAS Configuration

The RAS is a fiber-reinforced multilayer epoxy composite composed of three parts, as shown in Fig. 1:

1) an IA, made of a glass-fiber/epoxy multilayer composite;
2) a lossy laminate (LL), consisting of a multilayer composite made of GNP-coated glass fiber in an epoxy matrix;
3) a shieding back (SB), made of a carbon-fiber/epoxy multilayer composite or an aluminum panel.

The LL is produced as described in the following, via air spraying of a suspension of GNPs in a mixture of acetone and epoxy resin over the glass-fiber fabric. Successively,

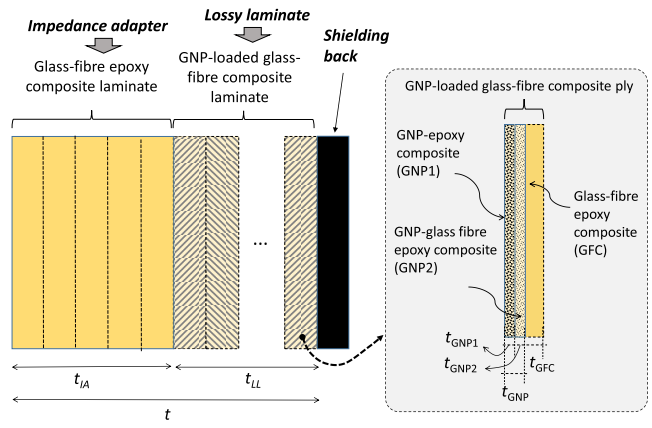

Fig. 1. Schematic configuration of the multilayered RAS composed by an IA, an LL, and a shielding back.

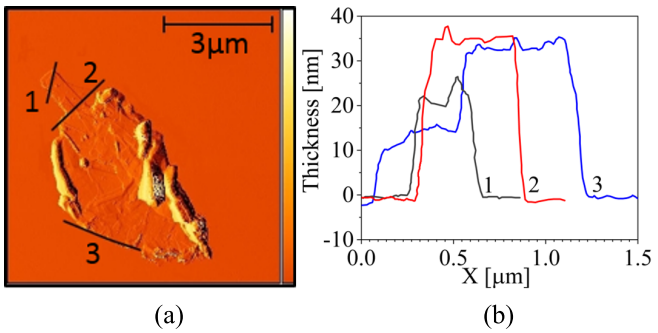

Fig. 2. AFM characterization of a single GNP flake. (a) Surface morphology. (b) Measured thickness profile.

the GNP-loaded glass-fiber fabrics are layered in order to produce the structural composite laminate through vacuum-assisted liquid resin infusion. In the resulting composite laminate, it results that each glass-fiber ply is composed of three layers: a GNP/epoxy coating, a GNP/glass fiber/epoxy composite, and a glass-fiber/epoxy composite (without GNPs), as shown in Fig. 1.

B. Materials

The resin used in this article is an aeronautical single-part epoxy, appropriately chosen for the injection process, with a curing time of 2 h at the temperature of 180 °C. Acetone with 99.9% of purity was purchased from Sigma-Aldrich Co., Ltd. The glass fiber fabric is a commercial product with a weight of 301 g/m^2 and a measured thickness of 235 ± 5 μm. The fabric consists of two layers of E-glass fiber supported on one another at ±45° sewn together with a polyester thread. GNPs used as filler are characterized by an average thickness of 30 nm and lateral dimensions from a few micrometers up to 10 μm, with an average value of 4.2 μm, as revealed from atomic force microscopy (AFM) investigations (see Fig. 2).

C. Fabrication of GNP-Filled LL

The composite laminates were produced through vacuum-assisted resin infusion [24], [25]. The glass fibers were previously prewetted with a GNP-filled sizing agent, and

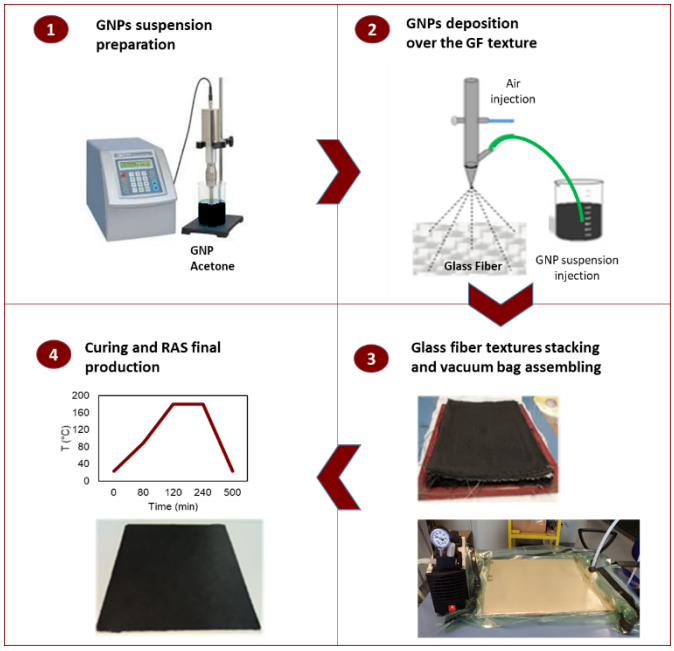

Fig. 3. Schematic of the production process.

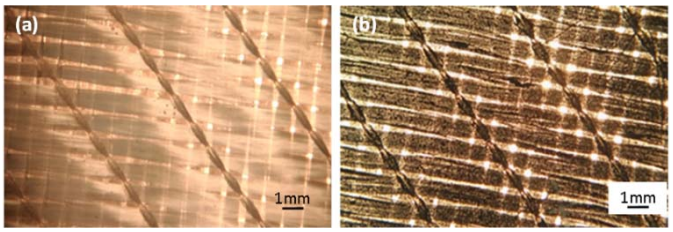

Fig. 4. Optical image of the glass-fiber fabric (a) without and (b) with GNP-filled sizing agent.

then, the plies were stacked in order to form a laminate. Next, the stacked plies were inserted in a vacuum bag and the composite laminate was produced applying the infusion system, as shown in Fig. 3.

Fig. 4 shows the optical images of the glass-fiber fabric before and after the deposition of the GNP-filled sizing agent. We notice a uniform distribution of the nanostructures over the fabric surface. The scanning electron microscopy (SEM) micrographs of Fig. 5 show the surface of the GNP-coated glass-fiber ply. It is evident that the GNP–epoxy sizing agent creates a thin layer of GNP-filled composite over the glass fiber texture and GNPs penetrate among fibers due to their small dimensions. It is noted that GNPs are present on both the surface and among fibers [see Fig. 5(a)]; this confirms the hypothesis that GNPs penetrate the glass-fiber texture within a depth of about 10 μm, comparable with the diameter of a fiber [see Fig. 5(b)].

Moreover, the good degree of adhesion between the resin filler and the fibers is shown in Fig. 5(c), where the resin-filler composite appears to be well bonded to the glass fiber substrate, even after the breakage in nitrogen. In the largest magnification [see Fig. 5(d)], there is the detailed view of the GNPs on the glass fibers.

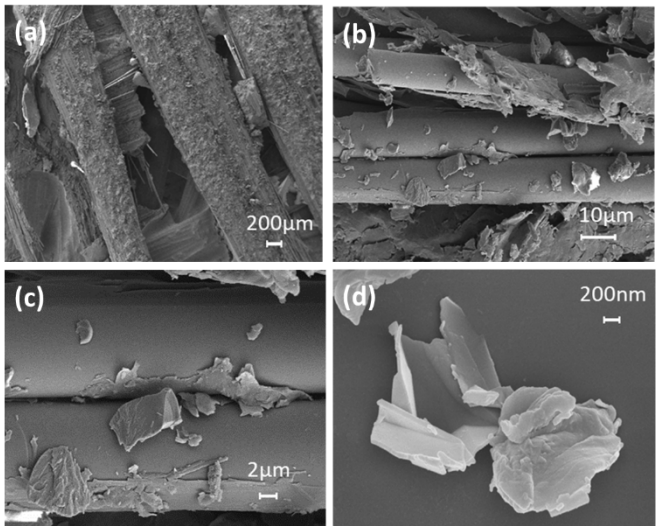

Fig. 5. SEM images. (a) Top surface of a glass fiber ply covered by the GNP-based sizing agent. (b) Fibers pull-out after breaking. (c) Integration between the glass fibers and GNP-based sizing agent. (d) Magnification of a GNP flake over a glass fiber.

Fig. 6 shows the cross section of the produced sample; it is observed that the most external layer of thickness t_{GNP1} is made of GNP–epoxy composite [see Fig. 6(a)]. In the following, there is the interlayer of glass-fiber/epoxy composite filled with GNPs, having thickness t_{GNP2}, which is followed by the third layer of plain glass-fiber/epoxy composite.

III. Design of Graphene-Filled RAS

The design of the RAS is performed by simulation, in the hypothesis of planar configuration and plane-wave normal incidence. To this purpose, the glass-fiber/epoxy composite (GFC) laminate, having the function of IA, is modeled as a uniform effective dielectric layer having thickness t_{IA} and effective dielectric permittivity ε_{GFC}. According to the experimental observation of Figs. 5 and 6, the LL is modeled as a cascade n_{LL} three layers made of a top layer of GNP/epoxy composite (GNP1), an interlayer of GNP/glass-fiber/epoxy composite (GNP2), and a bottom layer of glass-fiber/epoxy composite (GFC) (see Fig. 1). Each composite layer is modeled by applying the effective medium model described in Section III-D. The shielding back is made of perfect electric conducting material, and it is modeled as a zero-impedance surface.

A. Effective Medium Model of GNP-Coated Glass-Fiber/Epoxy Composite

Each layer of GNP-loaded glass-fiber/epoxy composite, shown in Fig. 7(a), is modeled through an effective medium approach as three homogeneous effective layers, according to the sketch of Fig. 7(b). The first layer (GNP1), having complex relative permittivity ε_{GNP1} and thickness t_{GNP1}, is the outer GNP/epoxy layer deposited over the glass-fiber texture. The second one (GNP2), having complex relative permittivity ε_{GNP2} and thickness t_{GNP2}, is representative of the GNP/glass-fiber/epoxy composite resulting from GNPs penetration among

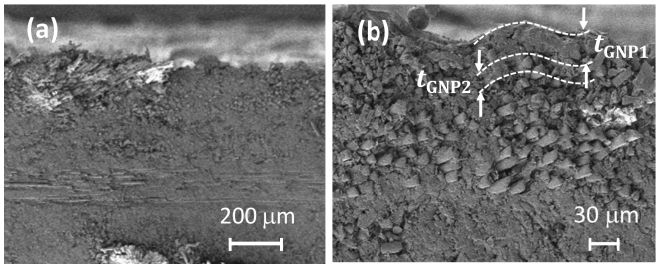

Fig. 6. SEM images of the cross section of the RAS at different magnifications.

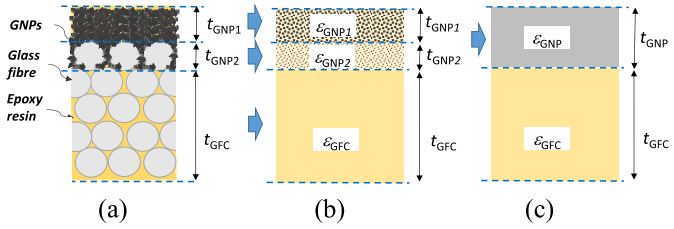

Fig. 7. Effective medium model of the graphene-loaded glass-fiber/epoxy composite layer.

the glass fibers. The third one (GFC), having complex relative permittivity ε_{GFC} and thickness t_{GFC}, is the part of the plain glass-fiber/epoxy composite without GNPs.

The relative complex permittivity of the glass-fiber/epoxy composite layer of thickness t_{GFC} is computed as

$$\varepsilon_{GFC} = \theta_{GF}\varepsilon_{GF} + (1 - \theta_{GF})\varepsilon_{epx} \tag{1}$$

in which θ_{GF} is the volume fraction of glass fiber and ε_{GF} and ε_{epx} are the relative dielectric permittivity of glass fiber and of epoxy resin, respectively. Assuming a glass fiber fabric with a glass content of 300 g/m^2, $\varepsilon_{GF} = 5.7$, and $\varepsilon_{epx} = 3$, it results $\theta_{GF} = 0.48$ and $\varepsilon_{GFC} = 4.3$. For a glass-fiber fabric with a glass content of 116 g/m^2, it results $\varepsilon_{GFC} = 3.5$.

The relative complex effective permittivity ε_{GNP1} of the GNP-filled composite layer of thickness t_{GNP1}

$$\varepsilon_{GNP1} = \varepsilon'_{GNP1} + j\varepsilon''_{GNP1} \tag{2}$$

is computed by applying the multiscale Maxwell Garnett (MMG) model described in [18], [20], and [22], as shown in Fig. 8, assuming that θ_{GNP} is the volume concentration of GNPs in the composite.

θ_{GNP} is expressed as a function of the total weight per square meter of GNPs dispersed in each ply of the RAS, P_{GNP}. At first, the total weight of GNPs dispersed in the top layer GNP1 is computed by

$$P_{GNP1} = P_{GNP}/[1 + (1 - \theta_{GF})(t_{GNP2}/t_{GNP1})]. \tag{3}$$

Therefore, the corresponding weight concentration of GNPs in the layer GNP1 with respect to resin is evaluated

$$x_{GNP1} = P_{GNP1}/(\delta_{epx} t_{GNP1}) \tag{4}$$

in which $\delta_{epx} = 1.19$ g/cm^3 is the density of the epoxy resin. The volume concentration of the GNPs in the layer GNP1 is then obtained as

$$\theta_{GNP1} = 1/[1 + (1/x_{GNP1})(\delta_{GNP}/\delta_{epx})] \tag{5}$$

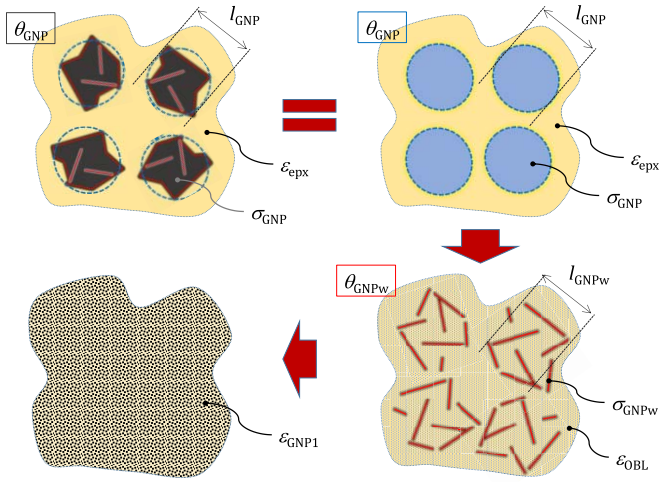

Fig. 8. Sketch of the MMG modeling of the GNP/epoxy composite GNP1.

in which δ_{GNP} is the density of the GNP powders. For GNPs of the dimensional class considered in this article, δ_{GNP} ranges from 0.2 to 0.4 g/cm^3, as reported in the datasheets of commercially available GNP powders (i.e., Sigma Aldrich 900439-250G, 900407-250G, and 900394-250 G).

The first step in the modeling of the GNP composite layer GNP1 consists in the calculation of the effective complex permittivity ε_{OBL} of an effective medium made of oblate ellipsoids, having as principal axes the average lateral dimension l_{GNP} and the average thickness d_{GNP} of the GNPs, dispersed in the epoxy resin with a volume concentration θ_{GNP}

$$\varepsilon_{OBL} = \varepsilon_{epx} + \frac{\varepsilon_{epx}\theta_{GNP1}\Phi}{3 - \theta_{GNP1}\Psi} \tag{6}$$

in which

$$\Phi = \frac{4}{2\kappa_{epx} + 1 - N_{OBL}} + \frac{1}{\kappa_{epx} + N_{OBL}} \tag{7a}$$

$$\Psi = \frac{2(1 - N_{OBL})}{2\kappa_{epx} + 1 - N_{OBL}} + \frac{N_{OBL}}{\kappa_{epx} + N_{OBL}} \tag{7b}$$

with

$$\kappa_{epx} = \frac{j\omega\varepsilon_0\varepsilon_{epx}}{j\omega\varepsilon_0(1 - \varepsilon_{epx}) + \sigma_{GNP}} \tag{8a}$$

$$N_{OBL} = \frac{\left(1 + e_{OBL}^2\right)\left[e_{OBL} - \tan^{-1}(e_{OBL})\right]}{e_{OBL}^3} \tag{8b}$$

$$e_{OBL} = \sqrt{\left(\frac{l_{GNP}}{d_{GNP}}\right)^2 - 1} \tag{8c}$$

where ω is the angular frequency. The oblate ellipsoids dispersed in the epoxy resin account for the effect of GNP–polymer interaction at the microscale.

The second step consists in the calculation of the effective complex permittivity of the GNP/epoxy layer, applying iteratively the Maxwell Garnett formula to the composite made of cylindrical rods of length l_{GNPw} and diameter d_{GNPw} proportional to the GNP's average thickness, with a volume concentration θ_{GNPw}, which is proportional to the GNP's volume concentration and an effective conductivity σ_{GNPw}

proportional to the GNP's one. The cylindrical roads are assumed to be dispersed uniformly in the effective medium of permittivity $\varepsilon_{\mathrm{OBL}}$. They represent the effect of nanoscale interaction, through sharp edges and wrinkles, between GNPs and polymer.

It results

$$\varepsilon_{\mathrm{GNP1}} = \varepsilon_{\mathrm{OBL}} + \frac{\varepsilon_{\mathrm{OBL}}\theta_{\mathrm{GNPw}}\Gamma}{3 - \theta_{\mathrm{GNPw}}\Delta} \tag{9}$$

in which

$$\Gamma = \frac{4}{2\kappa_{\mathrm{OBL}} + 1} + \frac{1}{\kappa_{\mathrm{OBL}} + N_{\mathrm{ROD}}} \tag{10a}$$

$$\Delta = \frac{2}{2\kappa_{\mathrm{OBL}} + 1} + \frac{N_{\mathrm{ROD}}}{\kappa_{\mathrm{OBL}} + N_{\mathrm{ROD}}} \tag{10b}$$

with

$$\kappa_{\mathrm{OBL}} = \frac{j\omega\varepsilon_0\varepsilon_{\mathrm{OBL}}}{j\omega\varepsilon_0(1 - \varepsilon_{\mathrm{OBL}}) + \sigma_{\mathrm{GNPw}}} \tag{11a}$$

$$N_{\mathrm{ROD}} = \left(\frac{d_{\mathrm{GNPw}}}{l_{\mathrm{GNPw}}}\right)^2 \ln\left(\frac{l_{\mathrm{GNPw}}}{d_{\mathrm{GNPw}}}\right). \tag{11b}$$

Finally, the relative complex permittivity $\varepsilon_{\mathrm{GNP2}}$ of the GNP/glass-fiber/epoxy composite layer of thickness t_{GNP2} is computed as

$$\begin{aligned}\varepsilon_{\mathrm{GNP2}} &= \theta_{\mathrm{GF}}\varepsilon_{\mathrm{GF}} + (1 - \theta_{\mathrm{GF}})\varepsilon_{\mathrm{GNP1}} \\ &= \varepsilon'_{\mathrm{GNP2}} + j\varepsilon''_{\mathrm{GNP2}},\end{aligned} \tag{12}$$

in which the real and imaginary parts $\varepsilon'_{\mathrm{GNP2}}$ and $\varepsilon''_{\mathrm{GNP2}}$ of the complex effective relative permittivity $\varepsilon_{\mathrm{GNP2}}$ are given by

$$\varepsilon'_{\mathrm{GNP2}} = \theta_{\mathrm{GF}}\varepsilon_{\mathrm{GF}} + (1 - \theta_{\mathrm{GF}})\varepsilon'_{\mathrm{GNP1}} \tag{13a}$$

$$\varepsilon''_{\mathrm{GNP2}} = (1 - \theta_{\mathrm{GF}})\varepsilon''_{\mathrm{GNP1}}. \tag{13b}$$

In the hypothesis that the two GNP-filled composite layers, GNP1 and GNP2, are electrically thin in the considered frequency range, the following conditions are satisfied:

$$\beta_{\mathrm{GNP}i}\, t_{\mathrm{GNP}i} \ll 1, \quad i = 1, 2 \tag{14}$$

in which β_{GNP1} and β_{GNP2} are the phase constants of the effective media GNP1 and GNP2

$$\beta_{\mathrm{GNP}i} = \frac{\omega}{c_0}\sqrt{\frac{\varepsilon'_{\mathrm{GNP}i}}{2}\left[1 + \sqrt{1 + \left(\frac{\varepsilon''_{\mathrm{GNP}i}}{\varepsilon'_{\mathrm{GNP}i}}\right)^2}\right]}, \quad i = 1, 2 \tag{15}$$

with $c_0 = 1/\sqrt{\mu_0\varepsilon_0}$. Therefore, the bilayer made of the two GNP-filled composite GNP1 and GNP2 can be modeled as an effective homogeneous single layer of thickness t_{GNP}

$$t_{\mathrm{GNP}} = t_{\mathrm{GNP1}} + t_{\mathrm{GNP2}} \tag{16}$$

and complex relative permittivity $\varepsilon_{\mathrm{GNP}}$ given by

$$\varepsilon_{\mathrm{GNP}} = \varepsilon_{\mathrm{GNP1}}\frac{t_{\mathrm{GNP1}}}{t_{\mathrm{GNP}}} + \varepsilon_{\mathrm{GNP2}}\frac{t_{\mathrm{GNP2}}}{t_{\mathrm{GNP}}}. \tag{17}$$

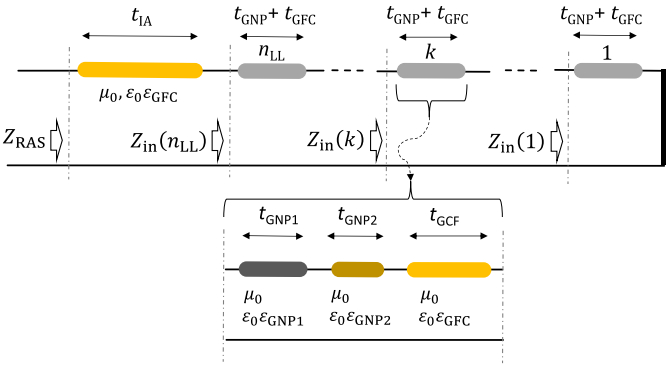

Fig. 9. Equivalent transmission-line model of the RAS.

B. Calculation of the RAS Reflection Coefficient

It is assumed that the RAS of Fig. 1 is illuminated by a plane wave with normal incidence. The reflection coefficient of the RAS is computed by applying the transmission-line formalism.

At first, the input impedance of the RAS illuminated by the plane wave is computed by considering the transmission-line model of the RAS, as shown in Fig. 9. It results

$$Z_{\mathrm{RAS}} = \eta_{\mathrm{GFC}}\frac{Z_{\mathrm{in}}(n_{\mathrm{LL}}) + \eta_{\mathrm{GFC}}\mathrm{tgh}(\gamma_{\mathrm{GFC}}t_{\mathrm{IA}})}{\eta_{\mathrm{GFC}} + Z_{\mathrm{in}}(n_{\mathrm{LL}})\mathrm{tgh}(\gamma_{\mathrm{GFC}}t_{\mathrm{IA}})} \tag{18}$$

in which η_{GFC} and γ_{GFC} are the intrinsic impedance and propagation constant, respectively, of the IA made of glass-fiber-reinforced composite having relative permittivity $\varepsilon_{\mathrm{GFC}}$

$$\eta_{\mathrm{GFC}} = \eta_0/\sqrt{\varepsilon}_{\mathrm{GFC}} \tag{19a}$$

$$\gamma_{\mathrm{GFC}} = j\omega\sqrt{\varepsilon}_{\mathrm{GFC}}/c_0 \tag{19b}$$

$\eta_0 = \sqrt{\mu}_0/\varepsilon_0$ being the free-space impedance, and $Z_{\mathrm{in}}(n_{\mathrm{LL}})$ is the input impedance of the lossy sheet made by the cascade of n_{LL} graphene-loaded glass-fiber composite layers.

Considering that each graphene-loaded glass-fiber composite layer is modeled as the cascade of three composite layers, having thicknesses t_{GNP1}, t_{GNP2}, and t_{GFC} [see Fig. 7(b)], $Z_{\mathrm{in}}(n_{\mathrm{LL}})$ is computed by applying the following recursive expressions:

$$Z_{\mathrm{in}}(k) = \eta_{\mathrm{GNP1}}\frac{Z_{\mathrm{GNP2}}(k) + \eta_{\mathrm{GNP1}}\mathrm{tgh}(\gamma_{\mathrm{GNP1}}t_{\mathrm{GNP1}})}{\eta_{\mathrm{GNP1}} + Z_{\mathrm{GNP2}}(k)\mathrm{tgh}(\gamma_{\mathrm{GNP1}}t_{\mathrm{GNP1}})} \tag{20a}$$

$$Z_{\mathrm{GNP2}}(k) = \eta_{\mathrm{GNP2}}\frac{Z_{\mathrm{GFC}}(k) + \eta_{\mathrm{GNP2}}\mathrm{tgh}(\gamma_{\mathrm{GNP2}}t_{\mathrm{GNP2}})}{\eta_{\mathrm{GNP2}} + Z_{\mathrm{GFC}}(k)\mathrm{tgh}(\gamma_{\mathrm{GNP2}}t_{\mathrm{GNP2}})} \tag{20b}$$

$$Z_{\mathrm{GFC}}(k) = \eta_{\mathrm{GFC}}\frac{Z_{\mathrm{in}}(k-1) + \eta_{\mathrm{GFC}}\mathrm{tgh}(\gamma_{\mathrm{GFC}}t_{\mathrm{GFC}})}{\eta_{\mathrm{GFC}} + Z_{\mathrm{in}}(k-1)\mathrm{tgh}(\gamma_{\mathrm{GFC}}t_{\mathrm{GFC}})} \tag{20c}$$

in which $k = (1; n_{\mathrm{LL}})$, and η_{GNP1}, γ_{GNP1}, η_{GNP2}, and γ_{GNP2} are the intrinsic impedances and propagation constants of the two GNP composite layers GNP1 and GNP2 in Fig. 7(b), having relative permittivity $\varepsilon_{\mathrm{GNP1}}$ and $\varepsilon_{\mathrm{GNP2}}$, respectively

$$\eta_{\mathrm{GNP}i} = \eta_0/\sqrt{\varepsilon}_{\mathrm{GNP}i}, \quad i = 1, 2 \tag{21a}$$

$$\gamma_{\mathrm{GNP}i} = j\omega\sqrt{\varepsilon}_{\mathrm{GNP}i}/c_0, \quad i = 1, 2. \tag{21b}$$

For $k = 1$, it is set to

$$Z_{\mathrm{in}}(0) = 0. \tag{22}$$

The reflection coefficient of the RAS in decibel is then given by the following expression:

$$R_{\mathrm{dB}} = 20\log_{10}\left|\frac{Z_{\mathrm{RAS}} - \eta_0}{Z_{\mathrm{RAS}} + \eta_0}\right|. \tag{23}$$

IV. Model Parameter Setting and Validation Through Experimental Testing

The model proposed in Section III was validated through experimental testing in order to define the values of the different parameters describing the electrical and morphological properties of the composite.

The values of the average lateral dimension and average thickness of the GNPs, $l_{\mathrm{GNP}} = 4.2$ μm and $d_{\mathrm{GNP}} = 30$ nm, were derived from SEM and AFM observations, as reported in Section II.

The average width d_{GNPw} and the average length l_{GNPw} of the wrinkles formed over the GNP surface by bending of the graphene flakes were set to 135 nm and 5.25 μm, respectively, as estimated from the SEM and AFM analyses.

The effective electrical conductivity of the GNPs σ_{GNP} and the GNP's wrinkles σ_{GNPw} was set to 20 and 6.4 kS/m, respectively, according to the results of previous studies [22].

The volume concentrations of the GNPs in the GNP–epoxy composite [i.e., top layer GNP1 in Fig. 7(b)] θ_{GNP1} and of the GNP's wrinkles θ_{GNPw} are estimated from effective permittivity measurements of reference test specimens, as described in the following.

A. Complex Permittivity Measurement

Let us consider a single ply of GNP-loaded glass-fiber/epoxy composite, as shown in Fig. 7. The relative effective complex permittivity $\varepsilon_{\mathrm{GNP}}$ of the homogeneous equivalent layer of thickness t_{GNP} in Fig. 7(c), defined by (17), was extrapolated from the transmission/reflection measurements according to the standard ASTM D5568 "Standard Test Method for Measuring Relative Complex Permittivity and Relative Magnetic Permeability of Solid Materials at Microwave Frequencies Using Waveguide," applying the deembedding technique described in [26]. To this purpose, the GNP-loaded effective composite layer of Fig. 7(c) is modeled as a two-port circuit, as shown in Fig. 10, with complex scattering parameters S_{11}, S_{22}, and $S_{12} = S_{21}$, which are obtained from the experimental tests.

Measurements of the scattering parameters are performed in the range 12.4–18 GHz (Ku-band) using the Anritsu Vector Star MS4647A vector network analyzer (VNA) and a WR-62 rectangular waveguide filled with a sample constituted by a single ply of GNP-loaded carbon-fiber composite and by three layers of GF-epoxy composites. A test sample was inserted in the aluminum flange of a WR-62 waveguide (15.8 mm × 7.9 mm) in size, having a thickness of about 2 mm.

The measured complex scattering parameters S_{ij}, $(i, j = 1, 2)$, of the filled flange, were corrected in phase in order to consider the air gaps between the sample surfaces and the calibrated reference planes and then recorded as a function of frequency. Then, the transmission parameters A, B, C, and D of the single ply of GNP-loaded composite are obtained from the measured scattering parameters

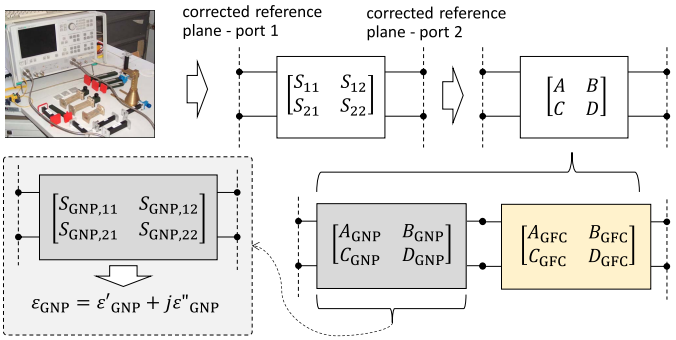

Fig. 10. Cascade connection of two-port network transmission matrices of GNP-based effective layer and GFC one.

$$A = \left[(1 + S_{11})(1 - S_{22}) + S_{21}^2\right]/(2S_{21}) \tag{24a}$$
$$B = \eta_{w0}\left[(1 + S_{11})(1 + S_{22}) - S_{21}^2\right]/(2S_{21}) \tag{24b}$$
$$C = \left[(1 - S_{11})(1 - S_{22}) - S_{21}^2\right]/(2\eta_{\mathrm{w0}}S_{21}) \tag{24c}$$
$$D = \left[(1 - S_{11})(1 + S_{22}) + S_{21}^2\right]/(2S_{21}) \tag{24d}$$

in which

$$\gamma_{\mathrm{w0}} = j\sqrt{\left(\omega c_0^{-1}\right)^2 - (\pi a^{-1})^2} \tag{25a}$$
$$\eta_{\mathrm{w0}} = j\omega\mu_0\gamma_{\mathrm{w0}}^{-1} \tag{25b}$$

are, respectively, the propagation constant inside the empty waveguide and the empty waveguide reference impedance, $a = 15.8$ mm being the major inner dimension of the cross section of the rectangular waveguide.

Next, the single ply of GNP-loaded composite is modeled as the cascade of two-port circuits with transmission parameters $A_{\mathrm{GNP}} = D_{\mathrm{GNP}}$, B_{GNP}, and C_{GNP} and $A_{\mathrm{GFC}} = D_{\mathrm{GFC}}$, B_{GFC}, and C_{GFC} and corresponding to the top GNP–epoxy composite layer of thickness t_{GNP} and to the bottom one made of plain glass-fiber/epoxy composite, having thickness t_{GCF} [see Fig. 7(c)]. It results

$$\begin{bmatrix} A & B \\ C & D \end{bmatrix} = \begin{bmatrix} A_{\mathrm{GNP}} & B_{\mathrm{GNP}} \\ C_{\mathrm{GNP}} & D_{\mathrm{GNP}} \end{bmatrix}\begin{bmatrix} A_{\mathrm{GFC}} & B_{\mathrm{GFC}} \\ C_{\mathrm{GFC}} & D_{\mathrm{GFC}} \end{bmatrix}. \tag{26}$$

The transmission parameters of the plain GFC layer in (26) are computed using the following analytical expressions:

$$A_{\mathrm{GFC}} = D_{\mathrm{GFC}} = \cosh(\gamma_{\mathrm{w,GFC}}t_{\mathrm{GFC}}) \tag{27a}$$
$$B_{\mathrm{GFC}} = \eta_{\mathrm{w,GFC}}\sinh(\gamma_{\mathrm{w,GFC}}t_{\mathrm{GFC}}) \tag{27b}$$
$$C_{\mathrm{GFC}} = \eta_{\mathrm{w,GFC}}^{-1}\sinh(\gamma_{\mathrm{w,GFC}}t_{\mathrm{GFC}}) \tag{27c}$$

in which

$$\gamma_{\mathrm{w,GFC}} = j\sqrt{\left(\omega c_0^{-1}\right)^2\varepsilon_{\mathrm{GFC}} - (\pi a^{-1})^2} \tag{28a}$$
$$\eta_{\mathrm{w,GFC}} = j\omega\mu_0\gamma_{\mathrm{w,GFC}}^{-1} \tag{28b}$$

are, respectively, the propagation constant and the wave impedance of the glass-fiber composite inside the waveguide, $\varepsilon_{\mathrm{GFC}}$ being the relative effective permittivity given by (1).

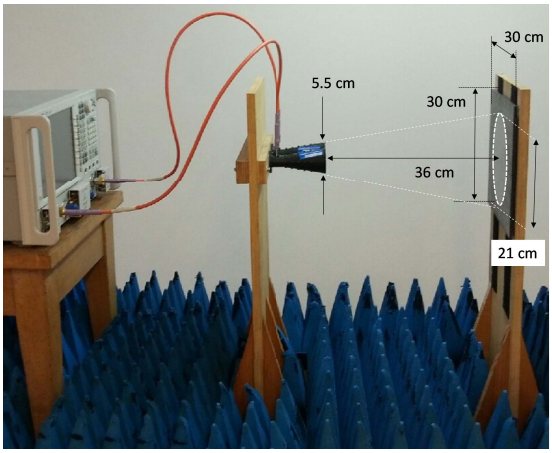

Fig. 11. Experimental test setup for reflection coefficient measurements. The (30 cm × 30 cm) test panel is positioned at the Fraunhofer distance of 36 cm from the horn antennas, having a diameter of ∼5.5 cm, and diameter of the power beam at −3 dB of 21 cm at the distance of 36 cm.

The transmission parameters of the GNP-filled composite layer are then obtained from (26)

$$A_{\mathrm{GNP}} = D_{\mathrm{GNP}} = AD_{\mathrm{GFC}} - BC_{\mathrm{GFC}} \tag{29a}$$

$$B_{\mathrm{GNP}} = -AB_{\mathrm{GFC}} + BA_{\mathrm{GFC}} \tag{29b}$$

$$C_{\mathrm{GNP}} = CD_{\mathrm{GFC}} - DC_{\mathrm{GFC}}. \tag{29c}$$

The scattering parameters of the GNP-loaded composite layer of thickness t_{GNP}, which is assumed to be uniform and homogeneous, are expressed as a function of the transmission parameters [see (29a)–(29c)]

$$S_{\mathrm{GNP},11} = S_{\mathrm{GNP},22} = \frac{B_{\mathrm{GNP}} - C_{\mathrm{GNP}}\eta_{\mathrm{w0}}^2}{2A_{\mathrm{GNP}}\eta_{\mathrm{w0}} + B_{\mathrm{GNP}} + C_{\mathrm{GNP}}\eta_{\mathrm{w0}}^2} \tag{30a}$$

$$S_{\mathrm{GNP},21} = S_{\mathrm{GNP},12} = \frac{2\eta_{\mathrm{w0}}}{2A_{\mathrm{GNP}}\eta_{\mathrm{w0}} + B_{\mathrm{GNP}} + C_{\mathrm{GNP}}\eta_{\mathrm{w0}}^2}. \tag{30b}$$

Finally, the modified iterative algorithm of Nicolson–Ross–Weir is applied in order to extract the effective complex permittivity $\varepsilon_{\mathrm{GNP}}$ of the GNP-loaded effective composite layer of Fig. 7(c) from the scattering parameters [see (30a) and (30b)].

B. Reflection Coefficient Measurement

The measurement of the reflection coefficient was performed in free space, in the frequency range of 6–18 GHz, by positioning the produced RAS panel having a dimension (30 cm × 30 cm) at the Fraunhofer distance of 36 cm from the aperture of the two-horn antennas used for measurements, as shown in Fig. 11. The two antennas, having a diameter of ∼5.5. cm, are connected to the input and output ports of a VNA (Agilent N5245A PNA-X) and operated in the bistatic mode. The power beam at −3 dB has a diameter of 21 cm at the Fraunhofer distance from the antennas so that scattering from the edges of the panel can be neglected.

The reflection coefficient measurements are performed for normal incidence, in both polarizations.

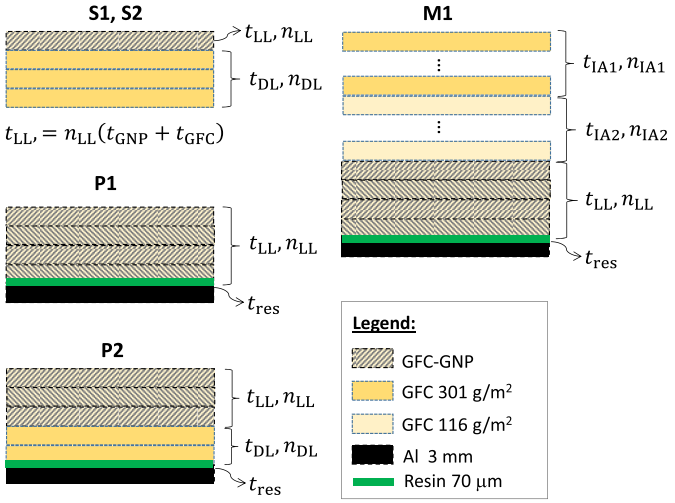

Fig. 12. Cross section of the produced specimens. S1 and S2 are used for effective permittivity measurement in a rectangular waveguide. P1 and P2 are (30 cm × 30 cm) multilayer panels without IA. M1 is a (30 cm × 30 cm) multilayer panel with IA.

V. Results

Different test specimens are produced in order to validate the proposed simulation model. Moreover, the modeling procedure is applied to the design of wideband RAS in the frequency range of 6–18 GHz. Fig. 12 shows the cross section of the produced samples, having the configuration reported in Table I.

Samples S1 and S2 are made of a single ply of GNP-loaded glass-fiber/epoxy composite and of three layers of plain GFRC with different contents of GNPs, i.e., respectively, 1 and 3 g/m^2 and are used for model validation and GNP-powder density estimation. Samples P1 and P2 are test panel (30 cm × 30 cm) in size. They are made of stacked glass-fiber/epoxy composite plies with a different GNP loading and are produced in order to validate the modeling and design procedure described in Section III. The RAS panel M1 is a wideband absorber with IA. A thin layer of epoxy resin of about 70 μm in thickness is used in order to glue the composite laminate to the aluminum panel realizing the shielding back.

The thicknesses of the different layers of the produced specimens and the total thickness are reported in Table I.

A. Validation of the Effective Medium Model of GNP–Epoxy Coating

The complex relative effective permittivities of the GNP-loaded glass-fiber composite layer of thickness t_{GNP} of samples S1 and S2 are obtained from scattering parameter measurements, applying the procedure described in Section IV. The measured real and imaginary parts of $\varepsilon_{\mathrm{GNP}}$ are reported as a function of the frequency in Fig. 13(a) and (b), respectively, for the specimens S1 and S2, loaded with GNPs at 1 and 3 g/m^2.

Next, the MMG model described in Section III is applied in order to simulate specimens S1 and S2 using the data reported in Table I. The value of the density of the GNP powders is

TABLE I

CHARACTERISTICS OF THE PRODUCED RAS SPECIMENS OF FIG. 12: GNP CONTENT, NUMBER OF PLIES, AND THICKNESSES

Specimen	GNP amount (g/m^2)	Number of plies				Thickness (μm)								
		n_{LL}	n_{DL}	n_{IA1}	n_{IA2}	t_{LL}	t_{GNP}	t_{GNP1}	t_{GNP2}	t_{DL}	t_{IA1}	t_{IA2}	t_{res}	t_{tot}
S1	1	1		-	-	270	50	39	11	720	-	-	-	990
S2	3	1		-	-	270	50	39	11	720	-	-	-	990
P1	3.25	4		-	-	1472	148	137	11	-	-	-	70	1542
P2	5	4	1	-	-	1088	52	41	11	240	-	-	70	1398
M1	5	4		6	4	1088	52	41	11	-	1000	1680	70	3838

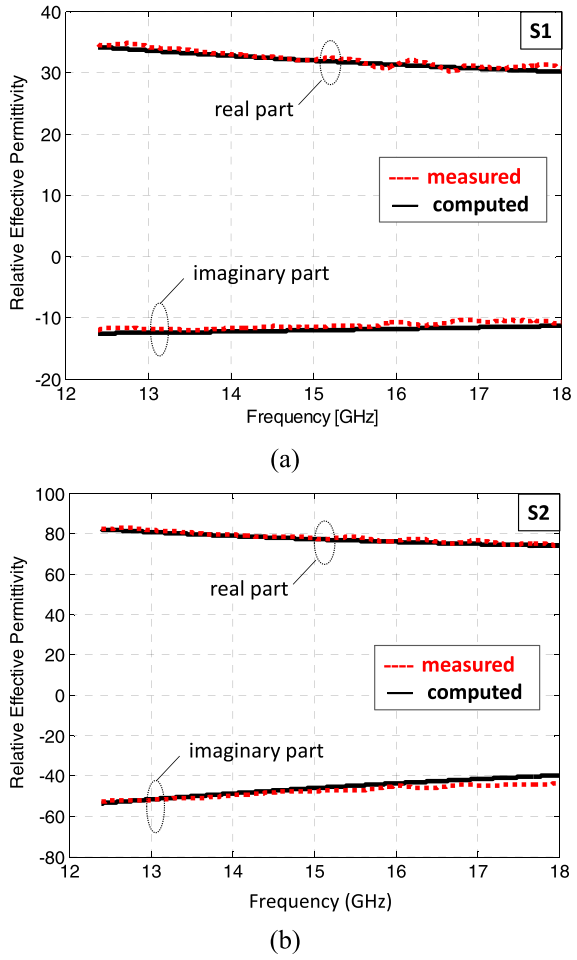

Fig. 13. Real and imaginary parts of the relative complex effective permittivity ε_{GNP} of samples (a) S1 and (b) S2, obtained from measurements and from calculations applying the MMG model mentioned in Section III.

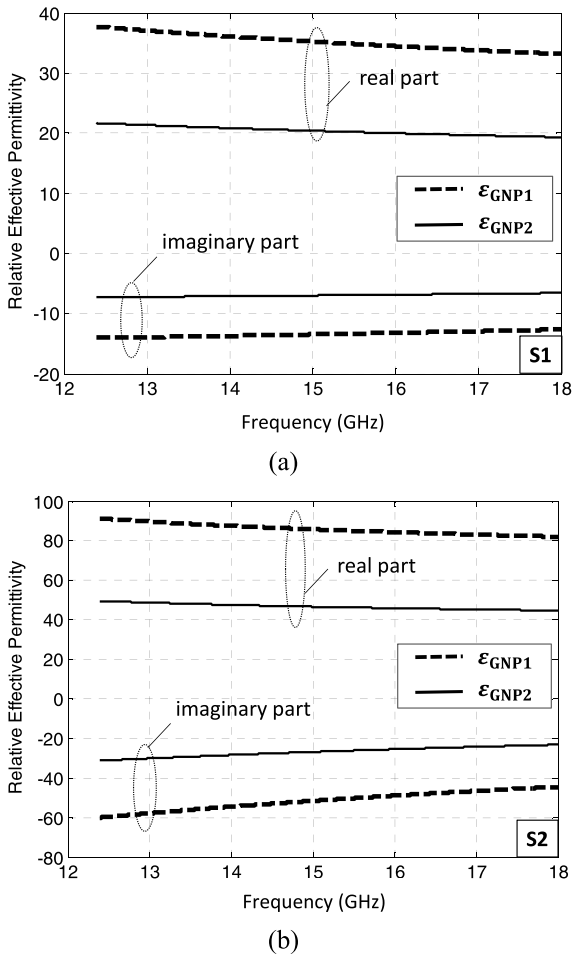

Fig. 14. Real and imaginary parts of the relative complex effective permittivities ε_{GNP1} and ε_{GNP2} of samples (a) S1 and (b) S2, obtained applying the MMG model mentioned in Section III, in the Ku-band.

extracted from (5) as

$$\delta_{GNP} = \delta_{epx} x_{GNP1}(1/\theta_{GNP1} - 1). \tag{31}$$

in which θ_{GNP1} is obtained from the best fit of the computed and measured complex effective permittivity ε_{GNP} and x_{GNP1} is given by (4). It results $\delta_{GNP} = 0.358$ g/cm^3, which is in line with the value reported in the datasheet of commercially available GNPs (i.e., 0.2–0.4 g/cm^3).

Therefore, the relative complex effective permittivities of the two layers in Fig. 7(c), of thickness t_{GNP1} and t_{GNP2}, respectively, are computed by applying the model described in Section III. The obtained results are reported in Fig. 14(a) and (b). Finally, expression (17) is applied in order to evaluate the complex effective permittivity ε_{GNP} of samples, as reported in Fig. 13(a) and (b). Notice a very good agreement between the computed and measured data, which demonstrates the validity of the proposed modeling approach.

B. EM Absorption Properties of the Produced RAS

Once the simulation model presented in Section III is validated and calibrated through the estimation of the GNP-powder density δ_{GNP}, the design of RAS for the X- and Ku-bands is performed.

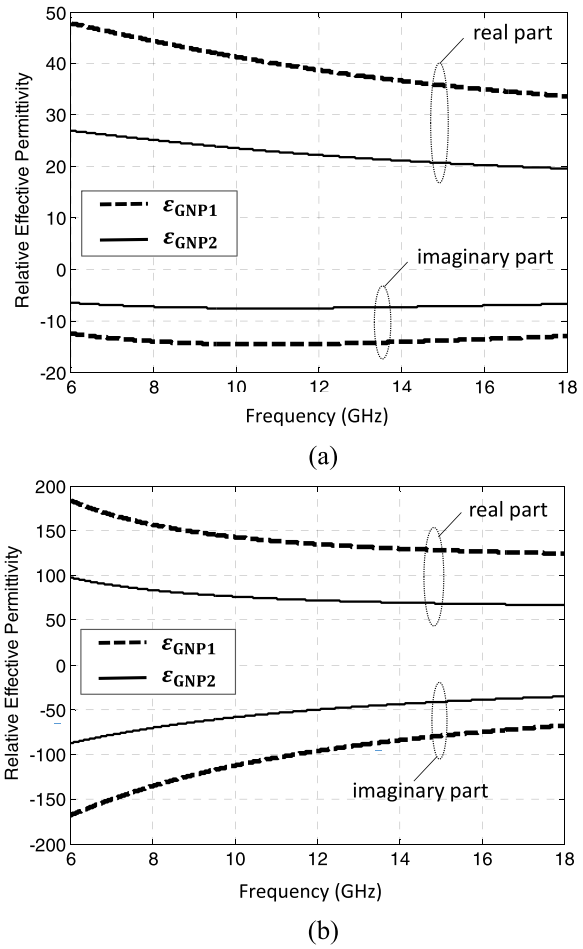

Fig. 15. Real and imaginary parts of the relative complex effective permittivities ε_{GNP1} and ε_{GNP2} computed for (a) P1 and (b) P2, in the 6–18 GHz frequency range applying the MMG model mentioned in Section III.

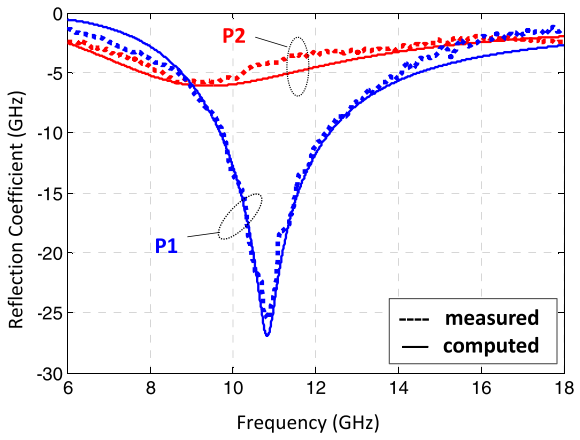

Fig. 16. Measured and computed reflection coefficients of the RAS panel P1 and P2 of Table I, without IA.

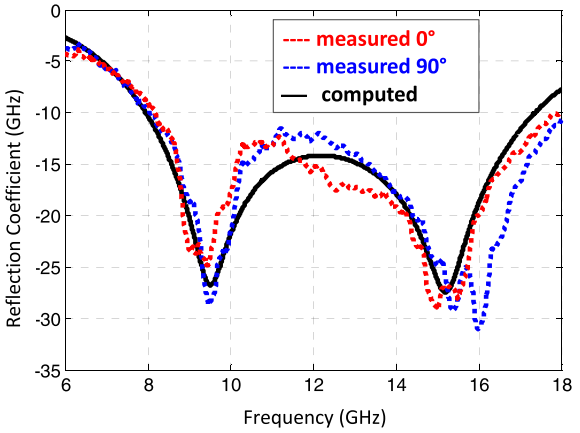

Fig. 17. Measured and computed reflection coefficients of the wideband RAS panel M1 of Table I, with IA.

At first, the two RASs in Table I without IA, i.e. P1, and P2, are designed, fabricated, and tested in free space, as described in Section II.

The relative effective permittivities of the GNP–epoxy composite top layer ε_{GNP1} and the GNP-filled glass-fiber composite ε_{GNP2} are computed by applying the model described in Section III. The computed frequency spectra are shown in Fig. 15(a) and (b).

The results of measured and computed reflection coefficient for normal incidence are reported in Fig. 16. We notice a very good agreement between measured and computed data, which confirms the validity of the proposed approach. The total thickness of the produced panel is 1.55 and 1.34 mm, respectively, with a frequency of minimum reflection of about 11 and 9 GHz, respectively.

In particular, panel P1, having a lower total content of GNPs distributed in thicker layers with respect to panel P2, is characterized by a minimum reflection of about −27 dB with a bandwidth at −10 dB of more than 2 GHz.

Then, the design of a wideband RAS is performed considering the configuration with IA, as shown in Figs. 1 and 12. Fig. 17 (continuous line) shows the reflection coefficient of the designed panel M1, having the characteristics reported in Table I, and a total thickness of 3.84 mm.

Next, the panel M1 is fabricated, as described in Section II. The laminated composite is glued over an aluminum flat panel having a thickness of 3 mm using a thin layer of epoxy resin, as shown in Fig. 12. The reflection coefficient of the panel M1 is measured in free space in the 0° and 90° polarizations, and the obtained data are reported in Fig. 17. We notice a good agreement between the measured and computed data. Some differences can be observed in the measured reflection coefficient for 0° and 90° polarizations, but this can be addressed to imperfections in the fabrication and assembly of the panel. The overall agreement, however, is satisfactory and demonstrates the validity of the proposed methodology.

The bandwidth at −10 dB of the reflection coefficient reaches 10 GHz and ranges from 8 up to 18 GHz. The minimum reflection reaches the value of −30 dB.

VI. Discussion

In order to demonstrate the novelty and relevance of the proposed technological approach for the design and production of wideband RAS, we made a performance comparison with the results presented in the literature in the last decade.

TABLE II

LITERATURE REVIEW AND PERFORMANCE COMPARISON OF RADAR-ABSORBING PANELS MADE WITH POLYMER NANOCOMPOSITES OR FSS OR GLASS-FIBER-REINFORCED COMPOSITES (GFRC) LOADED WITH CNTS OR GRAPHENE NANOSTRUCTURES

Ref.	Year	Structural panel (Yes/No); technology	$R_{\min}$ (dB)	Frequency range (GHz)	f_c (GHz)	$\Delta f_{@-10dB}$ (GHz)	t_{tot} (mm)	$\Delta f_{@-10dB}/f_c$ (%)	t_{tot}/λ_c (%)
[27]	2011	No; Nanocomposite	-30	8 - 12.4	10.2	~5	6.97	49%	24%
[28]	2015	No; FSS	-35.57	8 - 12.4	10.2	4.2	1.4	41%	5%
[29]	2018	No; FSS	-24.09	4 - 12.4	8.2	3.5	2.6	34%	9%
[5]	2006	Yes; GFRC laminate	-45	8 - 12.4	10.2	4.1	3.27	40%	11%
[6]	2015	Yes; GFRC laminate	-25	8 - 12.4	10.2	3.7	2.55	36%	9%
[30]	2012	Yes; GFRC laminate	-25	8 - 12.4	10.2	0.5	16.6	5%	56%
[31]	2015	Yes; GFRC laminate	-56	8 - 12.4	10.2	4	3.23	39%	11%
[24], 90° polarization	2018	Yes; GFRC laminate	-32	6 – 18	12	8.2	1	68%	4%
[24], 0° polarization	2018	Yes; GFRC laminate	-32	6 – 18	12	6.6	1	55%	4%
This work - panel M1	2019	Yes; GFRC laminate	-30	6 – 18	12	10	3.8	83%	15%

The wideband performance of a radar-absorbing panel is assessed considering the following parameters:

1) the bandwidth at −10 dB of reflection ($\Delta f_{@-10\,\mathrm{dB}}$) normalized to the central frequency (f_c) of the considered range;
2) the thickness of the panel (t_{tot}) normalized to the wavelength at the central frequency in free space (λ_c);
3) the minimum value of reflection coefficient ($R_{\min}$).

The results of the literature review and comparison with the performance of panels M1 produced in this article are reported in Table II. The first three references focus on RAM panels that are not designed for structural applications. Among them, we notice that the RAM, with the widest bandwidth at −10 dB of reflection is the one described in [27], which, however, has a thickness of about 24% of the wavelength at the central frequency of the considered range in free space. The best performances in terms of minimum thickness among the nonstructural panel are found in [28] and [29], which concerns frequency-selective surface (FSS) with narrowband absorbing performances. In all cases, the bandwidth at −10 dB is always smaller than 50%.

In the case of structural panels, we notice that the best performances in terms of minimum thickness are provided by the laminate described in [24], which, however, has a maximum bandwidth of 68% and is produced with glass fiber plies coated on both faces with GNP-filler prewetting agent.

The best performances in terms of absorption bandwidth are obtained with panel M1 developed in this article. We obtain a normalized bandwidth at −10 dB of 83%, which is an outstanding performance with respect to the state of the art, and it is quite unique considering that the thickness of the panel is only 15% of the wavelength at 12 GHz in free space.

VII. CONCLUSION

An innovative approach for the design and fabrication of laminated multilayered graphene-filled glass-fiber-reinforced composites having wideband EM absorption properties in the X- and Ku-bands is proposed. The new method consists in the spray deposition of GNPs directly on the glass-fiber fabrics and in the production of the laminated RAS through liquid resin infusion.

The proposed approach enables to produce broadband RAS with improved mechanical properties, as demonstrated in [24], and with a reflection coefficient always below −10 dB in the frequency range from 8 to 18 GHz, with a total thickness of 3.84 mm.

The design of the panel is performed applying an innovative multiscale effective medium modeling approach, which is validated experimentally through morphological observations of the produced material and measurements of the complex effective permittivity of the produced samples.

ACKNOWLEDGMENT

The authors would like to thank Dr. G. De Bellis for scanning electron microscopy analysis. The results of the VELOGRAF Project are the exclusive property of Leonardo S.p.A.

REFERENCES

[1] H.-K. Jang, J.-H. Shin, C.-G. Kim, S.-H. Shin, and J.-B. Kim, "Semi-cylindrical radar absorbing structures using fiber-reinforced composites and conducting polymers in the X-band," *Adv. Compos. Mater.*, vol. 20, no. 3, pp. 215–229, 2011.

[2] K.-Y. Park, S.-E. Lee, C.-G. Kim, and J.-H. Han, "Application of MWNT-added glass fabric/epoxy composites to electromagnetic wave shielding enclosures," *Compos. Struct.*, vol. 81, no. 3, pp. 401–406, 2007.

[3] I. M. De Rosa, F. Sarasini, M. S. Sarto, and A. Tamburrano, "EMC impact of advanced carbon fiber/carbon nanotube reinforced composites for next-generation aerospace applications," *IEEE Trans. Electromagn. Compat.*, vol. 50, no. 3, pp. 556–563, Aug. 2008.

[4] I. M. De Rosa, R. Mancinelli, F. Sarasini, M. S. Sarto, and A. Tamburrano, "Electromagnetic design and realization of innovative fiber-reinforced broad-band absorbing screens," *IEEE Trans. Electromagn. Compat.*, vol. 51, no. 3, pp. 700–707, Aug. 2009.

[5] S.-E. Lee, J.-H. Kang, and C.-G. Kim, "Fabrication and design of multi-layered radar absorbing structures of MWNT-filled glass/epoxy plain-weave composites," *Compos. Struct.*, vol. 76, no. 4, pp. 397–405, 2006.

[6] I. Choi, D. Lee, and D. G. Lee, "Radar absorbing composite structures dispersed with nano-conductive particles," *Compos. Struct.*, vol. 122, pp. 23–30, Apr. 2015.

[7] W.-K. Jung, B. Kim, M.-S. Won, and S.-H. Ahn, "Fabrication of radar absorbing structure (RAS) using GFR-nano composite and spring-back compensation of hybrid composite RAS shells," *Compos. Struct.*, vol. 75, nos. 1–4, pp. 571–576, 2006.

[8] J.-B. Kim, "Broadband radar absorbing structures of carbon nanocomposites," *Adv. Compos. Mater.*, vol. 21, no. 4, pp. 333–344, 2012.

[9] J.-H. Oh, K.-S. Oh, C.-G. Kim, and C.-S. Hong, "Design of radar absorbing structures using glass/epoxy composite containing carbon black in X-band frequency ranges," *Compos. B, Eng.*, vol. 35, no. 1, pp. 49–56, 2004.

[10] G. Lubineau and A. Rahaman, "A review of strategies for improving the degradation properties of laminated continuous-fiber/epoxy composites with carbon-based nanoreinforcements," *Carbon*, vol. 50, no. 7, pp. 2377–2395, 2012.

[11] A. Saib *et al.*, "Carbon nanotube composites for broadband microwave absorbing materials," *IEEE Trans. Microw. Theory Techn.*, vol. 54, no. 6, pp. 2745–2754, Jun. 2003.

[12] F. Meng *et al.*, "Graphene-based microwave absorbing composites: A review and prospective," *Compos. B, Eng.*, vol. 137, pp. 260–277, Mar. 2018.

[13] R. Umer, Y. Li, Y. Dong, H. J. Haroosh, and K. Liao, "The effect of graphene oxide (GO) nanoparticles on the processing of epoxy/glass fiber composites using resin infusion," *Int. J. Adv. Manuf. Technol.*, vol. 81, nos. 9–12, pp. 2183–2192, 2015.

[14] N. T. Kamar, M. M. Hossain, A. Khomenko, M. Haq, L. T. Drzal, and A. Loos, "Interlaminar reinforcement of glass fiber/epoxy composites with graphene nanoplatelets," *Compos. A, Appl. Sci. Manuf.*, vol. 70, pp. 82–92, Mar. 2015.

[15] R. K. Prusty, S. K. Ghosh, D. K. Rathore, and B. C. Ray, "Reinforcement effect of graphene oxide in glass fibre/epoxy composites at *in-situ* elevated temperature environments: An emphasis on graphene oxide content," *Compos. A, Appl. Sci. Manuf.*, vol. 95, pp. 40–53, Apr. 2017.

[16] A. K. Pathak, M. Borah, A. Gupta, T. Yokozeki, and S. R. Dhakate, "Improved mechanical properties of carbon fiber/graphene oxide-epoxy hybrid composites," *Compos. Sci. Technol.*, vol. 135, pp. 28–38, Oct. 2016.

[17] W. Qin, F. Vautard, L. T. Drzal, and J. Yu, "Mechanical and electrical properties of carbon fiber composites with incorporation of graphene nanoplatelets at the fiber–matrix interphase," *Compos. B, Eng.*, vol. 69, pp. 335–341, Feb. 2015.

[18] M. S. Sarto, A. G. D'Aloia, A. Tamburrano, and G. De Bellis, "Synthesis, modeling, and experimental characterization of graphite nanoplatelet-based composites for EMC applications," *IEEE Trans. Electromagn. Compat.*, vol. 54, no. 1, pp. 17–27, Feb. 2012.

[19] A. G. D'Aloia, M. D'Amore, and M. S. Sarto, "Adaptive broadband radar absorber based on tunable graphene," *IEEE Trans. Antennas Propag.*, vol. 64, no. 6, pp. 2527–2531, Jun. 2016.

[20] F. Marra *et al.*, "Electromagnetic and dynamic mechanical properties of epoxy and vinylester-based composites filled with graphene nanoplatelets," *Polymers*, vol. 8, no. 8, p. 272, 2016.

[21] C. L. Holloway, M. S. Sarto, and M. Johansson, "Analyzing carbon-fiber composite materials with equivalent-layer models," *IEEE Trans. Electromagn. Compat.*, vol. 47, no. 4, pp. 833–844, Nov. 2005.

[22] A. G. D'Aloia, F. Marra, A. Tamburrano, G. De Bellis, and M. S. Sarto, "Electromagnetic absorbing properties of graphene–polymer composite shields," *Carbon*, vol. 73, pp. 175–184, Jul. 2014.

[23] A. Rinaldi, A. Proietti, A. Tamburrano, and M. S. Sarto, "Graphene-coated honeycomb for broadband lightweight absorbers," *IEEE Trans. Electromagn. Compat.*, vol. 60, no. 5, pp. 1454–1462, Oct. 2018.

[24] F. Marra, J. Lecini, A. Tamburrano, L. Pisu, and M. S. Sarto, "Electromagnetic wave absorption and structural properties of wide-band absorber made of graphene-printed glass-fibre composite," *Sci. Rep.*, vol. 8, no. 1, Aug. 2018, Art. no. 12029.

[25] C. Lekakou, A. Hearn, A. K. Murugesh, and B. Le Page, "Liquid composite moulding of fibre nanocomposites," *Mater. Sci. Technol.*, vol. 23, no. 4, pp. 487–491, 2007.

[26] A. Tamburrano, F. Marra, J. Lecini, and M. S. Sarto, "Complex permittivity extraction method of a thin coating: EM properties of a graphene-based film on a composite layer," in *Proc. IEEE Int. Symp. Electromagn. Compat.*, Aug. 2018, pp. 602–607.

[27] D. Micheli *et al.*, "Broadband electromagnetic absorbers using carbon nanostructure-based composites," *IEEE Trans. Microw. Theory Techn.*, vol. 59, no. 10, pp. 2633–2646, Oct. 2011.

[28] R. Panwar, S. Puthucheri, V. Agarwala, and D. Singh, "Fractal frequency-selective surface embedded thin broadband microwave absorber coatings using heterogeneous composites," *IEEE Trans. Microw. Theory Techn.*, vol. 63, no. 8, pp. 2438–2448, Aug. 2015.

[29] V. K. Chakradhary, H. B. Baskey, R. Roshan, A. Pathik, and M. J. Akhtar, "Design of frequency selective surface-based hybrid nanocomposite absorber for stealth applications," *IEEE Trans. Microw. Theory Techn.*, vol. 66, no. 11, pp. 4737–4744, Nov. 2018.

[30] I. Choi, J. G. Kim, I. S. Seo, and D. G. Lee, "Radar absorbing sandwich construction composed of CNT, PMI foam and carbon/epoxy composite," *Compos. Struct.*, vol. 94, pp. 3002–3008, Sep. 2012.

[31] S.-W. Eun, W.-H. Choi, H.-K. Jang, J.-H. Shin, J.-B. Kim, and C.-G. Kim, "Effect of delamination on the electromagnetic wave absorbing performance of radar absorbing structures," *Compos. Sci. Technol.*, vol. 116, pp. 18–25, Sep. 2015.

Fabrizio Marra received the three-year degree in computer engineering, the master's degree in nanotechnology engineering, and the Ph.D. degree in materials engineering, technologies, and complex industrial systems from the Sapienza University of Rome, Rome, Italy, in 2009, 2012, and 2015, respectively.

During his Ph.D. degree, he was a Visiting Researcher with the Institute of Science and Technology of Polymers (CSIC-ICTP), Madrid, Spain. His scientific activity is mainly focused on the development of electromagnetic materials, absorbing radar materials, and deformation sensors. Since November 2016, he has been in service at the Department of Astronautics, Electrical and Energy Engineering (DIAEE), Sapienza University of Rome, and the Research Center on Nanotechnology Applied to Engineering CNIS, as the Technical Manager of the Reology Laboratory and Electroreology. He is currently a Research Fellow with the Department of Astronautics, Electrical and Energy Engineering, Sapienza University of Rome, and CNIS.

Julian Lecini received the M.Sc. degree in nanotechnology engineering from the Sapienza University of Rome, Rome, Italy, in 2017.

He collaborated with the Department of Astronautics, Electrical and Energy Engineering, Sapienza University of Rome, during the master's thesis period in order to develop nanostructured composites for RAM applications.

Alessio Tamburrano (M'02–SM'17) received the Laurea degree (*summa cum laude*) in electrical engineering, the master's degree in electromagnetic compatibility and environmental impact of electromagnetic fields, and the Ph.D. degrees in electrical engineering from the Sapienza University of Rome, Rome, Italy, in 2003, 2005, and 2007, respectively.

He was appointed as an Assistant Professor of electrotechnics at the Sapienza University of Rome in 2006, where he has been an Associate Professor of electrical engineering since 2018. His scientific production includes two chapter's contributions in books. He is the coauthor of five Italian patents (three internationalized). His current research interests include modeling, design, and experimental characterization of nanostructured and multifunctional materials for electromagnetic applications; development of graphene-based highly sensitive piezoresistive paints/coatings and porous nanocomposites with strain sensing capabilities for structural health monitoring and wearable electronics applications; and modeling and simulation of the transmission-line performances and signal integrity of nanointerconnects made of single-wall carbon nanotube bundles, multiwall carbon nanotubes, and graphene nanoribbons for future high-speed electronics. Such research activity has led to the publication of more than 90 articles in international journals and proceedings of international symposia.

Dr. Tamburrano received several awards from IEEE. From 2013 to 2017, he served as the Chair of the Technical Committee of the IEEE EMC Society TC-11 "Nanotechnology and Advanced Materials." From 2010 to 2014, he was the Project Leader of the Joint Project Team 80004-9—Nanotechnologies—Vocabulary—Part 9: Electrotechnical products and systems of the International Electrotechnical Commission (IEC). Since 2016, he has been a member of the Working Group P 2715—IEEE guides for the characterization of the shielding effectiveness of planar materials.

Maria Sabrina Sarto (M'93–SM'98–F'10) received the Ph.D. degree in electrical engineering from the Sapienza University of Rome, Rome, Italy, in 1997.

Since 2005, she has been a Full Professor of electrotechnics and electromagnetic compatibility with the Faculty of Engineering, Sapienza University of Rome. She was the Director of the Research Center on Nanotechnology Applied to Engineering from 2006 to 2015, and the Nanotechnology and Nanoscience Laboratory from 2010 to 2016. She has been the Director of the EMC and Nanotech Laboratory, DIAEE, since 1998. She has been the Pro-Rector for research infrastructures at the Sapienza University of Rome since 2015 and the Director of the Department of Astronautics, Electrical and Energy Engineering (DIAEE) since 2016. She has published more than 180 articles in the field of electromagnetic compatibility (EMC), nanotechnology, numerical electromagnetics, advanced materials for EMC, graphene-based radar-absorbing materials, and graphene-based strain sensors.

Dr. Sarto was a member of the Advisory Board of the IEEE Council on Nanotechnology. She was the Co-Chair of the IEEE EMC Society TC11 on "Nanotechnology and Advanced Materials," the Chair of the working group IEEE STD 299.1 of the IEEE EMC Society, and the General Co-Chair of the IEEE NANO 2015 and EMC EUROPE 2020. She was a Distinguished Lecturer of the IEEE EMC Society from 2001 to 2002. She was an Associate Editor of the IEEE TRANSACTIONS ON ELECTROMAGNETIC COMPATIBILITY from 1998 to 2017.